

# Submicron giant magnetoresistive sensors for biological applications

D.K. Wood\*, K.K. Ni, D.R. Schmidt, A.N. Cleland

*Department of Physics, University of California at Santa Barbara, Santa Barbara, CA 93106, USA*

Received 12 May 2004; received in revised form 15 July 2004; accepted 30 October 2004

Available online 8 December 2004

## Abstract

We have fabricated submicron giant magnetoresistive (GMR) structures and evaluated their sensitivity for biomagnetic applications. GMR devices were fabricated using electron beam lithography, with minimum dimensions below 100 nm. We developed a new characterization technique for these sensors, using a scanned nanoscale magnetic probe and monitoring the resulting response of the sensors. The magnetic field from the scanned probe is similar to that generated by the magnetic particles used to tag bioanalytes. The devices demonstrated extremely high magnetic field resolution. Noise measurements, combined with a local field sensitivity from the scanned probe measurements, predict a sensitivity of  $2 \times 10^{-16}$  emu/Hz<sup>1/2</sup> for a magnetic particle 100 nm above the sensor surface. This corresponds to detection of single 100 nm commercially available magnetic labels, which are the lowest size scale of labels now used in biological studies, with a signal-to-noise of unity. Additionally, we predict detection of single 200 nm magnetic labels with a position sensitivity of 93 nm/Hz<sup>1/2</sup>, allowing proximity detection for particles not directly bound to the sensor surface, with a corresponding signal-to-noise of 10.

© 2004 Elsevier B.V. All rights reserved.

*Keywords:* Giant magnetoresistance; Nanoscale sensor; Electron beam lithography; Biomagnetic label; Biosensor array; Magnetic field sensor

## 1. Introduction

Since the discovery of the giant magnetoresistive (GMR) effect in magnetic multilayer systems [1], sensors employing this effect have been utilized in many areas of science and technology. The potential application of these devices to the fields of biology and biophysics, however, is only just beginning to be realized. It has been proposed that the high sensitivity of GMR sensors to small magnetic fields could be employed for detection of biomolecules that have been tagged with magnetic labels [2,3]. GMR sensors are favored over competing optical detection schemes due to their higher sensitivity, lower background, compact size, and easy integrability with existing semiconductor electronics [3–5]. Such technology has implications in many areas of biological and medical research, including disease detection, treatment, and prevention [6–9]. Various schemes for implementing biosensors based on GMR technology have been explored [2,10,5]. The

sensitivity of a GMR sensor increases with decreasing sensor volume, while the number of biomolecules bound to the sensor surface, and thus the available signal, increases with increasing surface area. Thus a large array of small, tightly spaced sensors optimizes these two quantities for maximum sensitivity [2]. While devices on the size scale investigated here have been used in magnetic storage as well as in magnetic random access memory (MRAM) applications, devices investigated for biosensing, to date, have only been fabricated at the 1 μm scale and above. In this study, we investigate the response of submicron-scale GMR devices to magnetic fields in the range of those required for biological sensing. Such small-scale devices will increase the sensitivity to magnetically tagged analytes, and allow for more tightly packed sensors, increasing the overall responsivity. In addition, here we describe a unique technique for characterizing the response of GMR sensors, using a scanned magnetic probe that generates a highly local magnetic field with a spatial distribution and field strength similar to that expected in biomagnetic applications. We also describe a model that quantitatively reproduces the main features of the observed response.

\* Corresponding author. Tel.: +1 8058935421; fax: +1 8058938170.

E-mail address: [dkwood@umail.ucsb.edu](mailto:dkwood@umail.ucsb.edu) (D.K. Wood).

## 2. Methods

Our devices were fabricated from a GMR multilayer structure provided by a commercial vendor [11]. The active structure of the GMR material studied here, from the bottom-up is as follows (all thicknesses in Å):  $3 \times (\text{NiFeCo } 40/\text{CoFe } 15/\text{CuAgAu } 16/\text{CoFe } 15)/\text{NiFeCo } 40$ . The bulk material had a sheet resistance of  $75 \Omega/\square$  and a GMR response of 13% at the saturation field of 300 Oe (see Fig. 1). Our devices comprised single straight wires etched from the bulk GMR material. The devices were patterned using standard electron-beam lithography, using a bilayer lift-off resist structure, to define a dielectric dry-etch mask. Unwanted GMR material, unprotected by the etch mask, was then removed by chemically assisted ion beam etching using a 3 cm Kaufmann  $\text{Ar}^+$  ion mill [12]. The etch was performed with a 10 mA  $\text{Ar}^+$  beam at 400 V, while flowing 4 sccm of  $\text{Cl}_2$  across the sample surface. We measured a large number of devices, all with similar response characteristics. The four devices reported here were all 2  $\mu\text{m}$  in length, with widths of 100, 150, 250, and 400 nm (see Fig. 1). Electrical contact was made via Au wire bonds to optically defined Cr/Au bond pads, 5/100 nm in thickness, deposited by lift-off. It should be noted that similar device dimensions could be achieved using optical lithography, allowing this approach to be easily scaled to large sensor arrays.

We characterized the devices using both 4-wire resistance and 2-wire Wheatstone bridge measurements. The resistances of the 100, 150, 250, and 400 nm wires in the antiparallel magnetic states were 14.4 k $\Omega$ , 1.62 k $\Omega$ , 501  $\Omega$ , and 417  $\Omega$ , respectively. The resistance of the smallest device is higher than indicated by the sheet resistance and linewidth, probably because the film thickness was reduced during the etch. All devices showed a strong GMR response.

To simulate the presence of a magnetically tagged biomolecular analyte in the vicinity of the GMR device, we developed a technique in which a magnetized scanning probe microscope (SPM) tip was scanned over the surface of the patterned device while monitoring the device's electrical response. Scanned line images and two-dimensional

maps, representing magnetic response as a function of tip position, could be generated in this way. We used a Digital Instruments multi-mode scanning probe microscope (SPM) equipped with a magnetic tip [13]. The magnetic material on the SPM tip was a  $\sim 50$  nm CoCr film. Similar SPM tips have been shown by McVitie to have a near field response well approximated by a single dipole, aligned along the tip axis with a magnetic moment of  $5 \times 10^{-12}$  emu and a dipole-to-sample distance of 300 nm [14]. We note that in the far field region, magnetic SPM tips do not behave as magnetic dipoles because of extended magnetic material. On the size scale of the sensors reported here, however, the peak responses are only recorded for near field region, where the dipole fit is nearly exact. The fields from a dipole of this size are comparable to those from 2  $\mu\text{m}$  biomagnetic beads (Micromer-M) [15], which are commonly used in biomagnetic applications. The distance of the dipole to the surface is similar to the passivation layer thicknesses used in recent experimental biomagnetic demonstrations [5].

Measurements were made with the SPM [13] operating in both contact and tapping modes. Similar response patterns were seen in both modes; here we report only measurements made in tapping mode. We note that the distance of the dipole center from the end of the SPM tip is significantly larger than the tapping mode amplitude, so the similarity in response to both modes is not surprising. Resistance measurements were made using a balanced Wheatstone bridge. The bridge was balanced using a variable resistor with a resolution of 1  $\Omega$ , and was excited with a 1 V, 1.227 kHz signal, generating a  $I_B = 20 \mu\text{A}$  current through the GMR sample. The bridge error signal was read out using a lock-in amplifier, and 2D images as well as linescans were formed from the signal using the SPM software (see Fig. 2).

## 3. Results and discussion

All devices displayed a response to the scanned magnetic probe. Line scans, showing resistance as a function of magnetic probe position, are shown in Fig. 3. The line scans shown

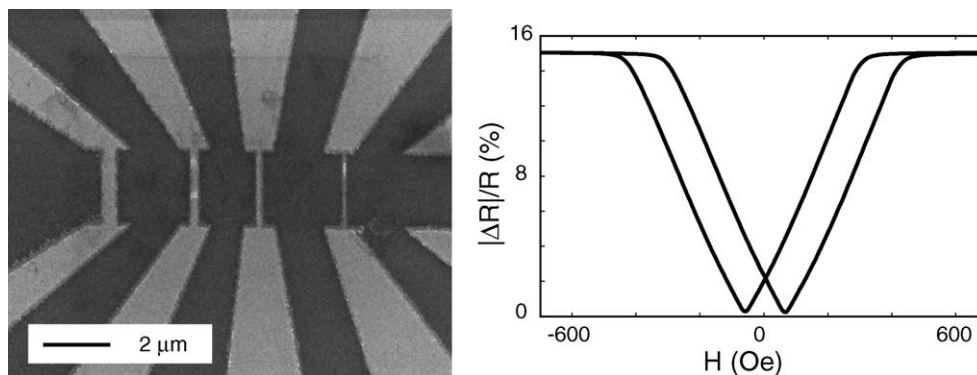


Fig. 1. Left: electron micrograph of four devices. The active region comprises the narrow wires in the center. Right: response of the bulk material at 300 K. The maximum  $|\Delta R|/R$  was 13%, which corresponds to an overall decrease in resistance at high fields, and the saturation field was 300 Oe.

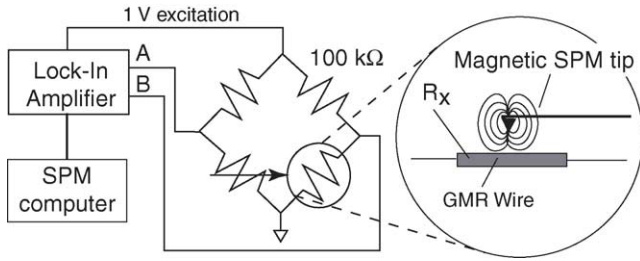


Fig. 2. Bridge circuit integrated with SPM hardware to allow measurement of GMR response as a function of tip position.

here were taken with the tip scanning perpendicular to the sensor long axis, near the device center line; scan rates were 0.5 Hz per pass. The peak fractional resistance changes for the 400, 250, and 150 nm devices were 0.25, 0.31, and 0.15%, respectively. The spatial resolution is seen to be a small fraction of the linewidth, with a 10–90% change in  $|\Delta R|/R$  occurring for a 250 nm displacement for Fig. 3(c), thus showing the highly local nature of the magnetic response. The 100 nm device showed a peak fractional change of only  $2.5 \times 10^{-5}$ , two orders of magnitude less than the other devices. The scans display the strong response of the devices to the tip field as the tip moved over the device. In addition, a hysteretic response is visible as a shift of the curve maximum as a function of tip position between the scan trace and retrace. The significantly smaller response observed for the 100 nm wide line is likely due to significant etch-induced thinning of the GMR structure, visible in the topographic image of devices made with that linewidth (not shown).

In order to better understand the imaged data from the devices, we created a simple model for the sensor response based on scanning an ideal magnetic dipole over a GMR sample modelled as a resistor network. In the model, we assumed that each device was composed of a network of smaller GMR sensors of unit area, shown Fig. 4(a). The network consisted of lines of series-connected GMR resistors, connected in par-

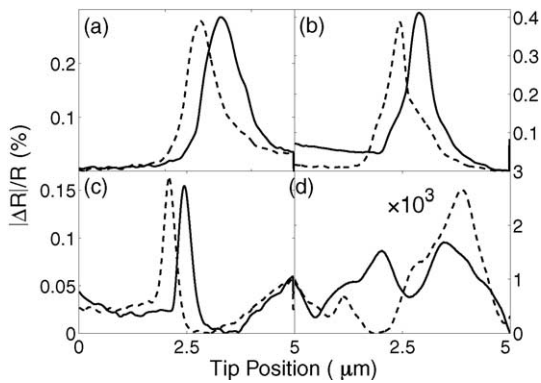


Fig. 3. Resistance change for magnetic SPM tip trace (solid line) and retrace (dashed line). Data are shown for (a) 400 nm, (b) 250 nm, (c) 150 nm, and (d) 100 nm devices; note scale change for the last. The peaks are close to the geometric center of the etched lines. Line scans were taken near the midpoint of the sensor long axis.

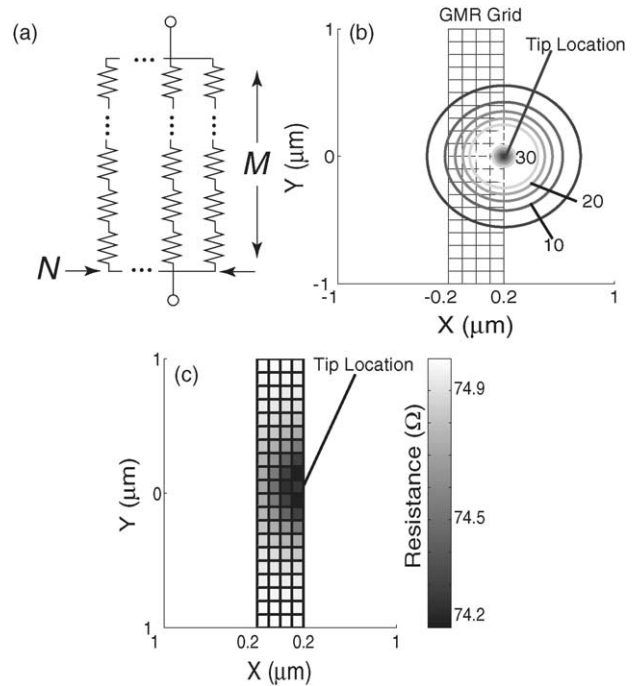


Fig. 4. GMR sensor model. (a)  $N \times M$  resistor network, with each resistor element an independent GMR sensor. (b) Contour plot of field generated from the tip in the plane of the sensor (contour lines are scaled linearly and labelled in Oe). The tip fields are overlaid with a  $4 \times 20$  resistor network, representing a  $0.4 \mu\text{m} \times 2 \mu\text{m}$  device. (c) Resistance values in network calculated from field in (b). Each grid cell represents an individual resistor in the  $4 \times 20$  network.

allel at either end of the device. In the calculations, we divided each sensor into  $N \times M$  smaller resistors, with  $N \times M$  changing for each sensor size, but always being on the order of 8000. These small resistors had a resistance equal to one square of the bulk GMR material, and were assumed to respond according to the static field curves for the bulk material, including the nonlinear responses at large field amplitudes shown in Fig. 1(b), but ignoring the hysteresis. The response of the patterned GMR sensor was simulated by choosing a tip location, calculating the tip field at the location of each resistor element, and then calculating the network resistance from the circuit model. We note that the variation in resistance due to the GMR effect is small enough that this simple model is reasonable.

The field from the tip was approximated by the dipole model developed by McVitie et al. [14], as mentioned above, with the dipole perpendicular to the plane of the sensor. We note that this dipole orientation corresponds to the most common magnetic label orientation used for biosensing. GMR sensors are far more sensitive to an in-plane field, so that an external field oriented perpendicular to the sensor plane, used to magnetize the magnetic labels, does not significantly affect the sensor response.

Because of the sensors' high sensitivity to an in-plane field, we have included only the in-plane components of the

tip's dipole field in our analysis, given by

$$H(x, y) = 3m_z h \frac{((x-d)^2 + y^2)^{1/2}}{((x-d)^2 + y^2 + h^2)^{5/2}} \quad (1)$$

in cgs units, where  $m_z$  and  $h$  are the dipole moment and height above the sensor plane, respectively, and  $(x, y)$  the in-plane coordinates, with origin at the sensor midpoint and  $y$  oriented along the sensor axis;  $z = 0$  is the sensor plane. The dipole is located a distance  $d$  from the sensor axis, and varies along the line scan. Fig. 4(b) shows a contour plot of the in-plane components of the field, for a  $m_z = 1 \times 10^{-12}$  emu dipole, positioned  $h = 300$  nm above the sensor surface, a distance  $0.2 \mu\text{m}$  from the device center line. The field contours are overlaid on a  $4 \times 20$  resistor network, representing a  $400$  nm device. In Fig. 4(c) we display the calculated response of each square of the resistor to this field.

In order to match the model to our measurements, we adjusted the dipole moment  $m_z$  and dipole height  $h$  for better quantitative agreement with the data. We performed a least squares analysis for the  $400$  nm device, minimizing the sum-squared-error between the model resistance and the observed data over the scan. This fit resulted in a magnetic moment  $m_z = 1.4 \pm 0.2 \times 10^{-12}$  emu and a dipole height,  $h = 430 \pm 3$  nm, in reasonable agreement with McVitie et al. [14]. Fig. 5 shows a comparison of the calculation and the data, for both the  $250$  nm and the  $400$  nm device. The width, height and shape of the peaks are quantitatively similar for both experiment and the model. The peak response measured for the  $400$  nm device is within 11% of the calculated response, and that for the  $250$  nm device agrees to within 35%.

The  $100$  and  $150$  nm devices had significantly weaker responses, so that the model gives good qualitative agreement but poorer quantitative agreement. To improve the quantitative fit, we measured the response of these particular devices to a uniform field, rather than using the bulk response to a uniform field in the model. Fig. 6(a) shows the response of the  $150$  nm device to a uniform field. Using the device geometry, we extracted the unit square response, and used this

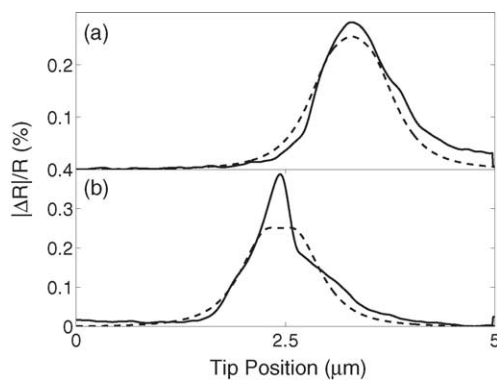


Fig. 5. Model calculation results for (a)  $400$  nm device and (b)  $250$  nm device, with  $N \times M$  equal to  $40 \times 200$  and  $30 \times 240$ , respectively. Solid curve is the measurement, dashed curve is model.

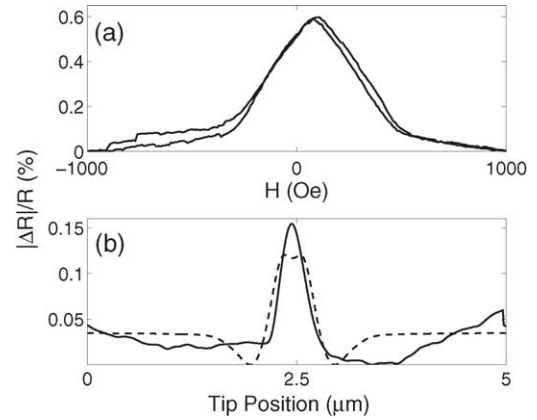


Fig. 6. Model calculations for  $150$  nm device. (a) Response of  $150$  nm device to uniform field oriented in-plane along long axis of sensor. (b) Results of model calculation for  $150$  nm device using data from (a) instead of bulk response data. Model calculations were made using a resistor network with  $N \times M$  equal to  $20 \times 260$ . Solid curve is the measurement, dashed curve is the model.

in the model calculations, with results shown in Fig. 6(b). These results display good quantitative as well as qualitative agreement between the model and the data. The fit for the  $100$  nm data did not improve significantly, we believe in part because the etch-induced damage made this sensor respond anomalously.

We measured the noise in the  $150$  nm linewidth device, shown in Fig. 7. Power spectra were measured with the bridge biased with a  $1$  V excitation, as well as unbiased. The latter contains only voltage noise power from the amplifier and resistor, while the former also includes resistance noise, which, due to the excitation current, modulates the detected voltage. The difference of the two power spectra, in Fig. 7(b), includes only the resistance noise, which is seen to be  $1/f$  to the upper limit of  $1$  kHz. In fact, the  $1/f$  part of the total spectral noise power Fig. 7(a) is dominated by the resistance noise. The white noise corresponds to a resistance noise of  $2.5 \times 10^{-3} \Omega/\sqrt{\text{Hz}}$ . The  $1/f$  resistance fluctuations correspond to  $0.015 \Omega/\sqrt{\text{Hz}}$ , measured at  $1$  Hz, with a slope  $1/f^\alpha$

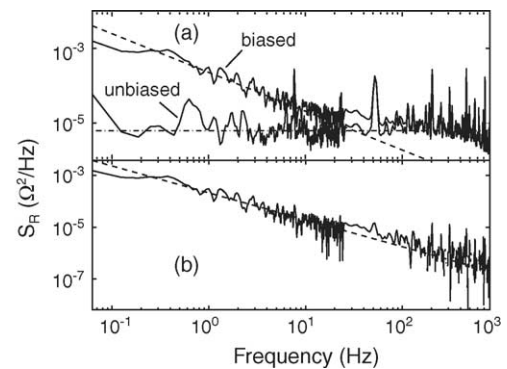


Fig. 7. Measured noise for  $150$  nm device, plotted in units of resistance noise power  $S_R = (1/I_B)^2 S_V$ , where  $S_V$  is the measured voltage noise and  $I_B = 20 \mu\text{A}$  the bias current. (a) Noise power with bridge biased and unbiased. (b) Difference of biased and unbiased noise powers. Dashed line is fit to  $1/f$  noise power, dashed-dotted line fit to white noise.

where  $\alpha = 0.88$ . The  $1/f$  noise can be avoided in a sensor application by modulating an external magnetic field above the  $1/f$  knee frequency at about 50 Hz. With a field sensitivity of  $21 \text{ m}\Omega/\text{Oe}$ , the white noise level corresponds to a uniform field sensitivity of  $120 \text{ mG}/\sqrt{\text{Hz}}$ . This is approximately an order of magnitude larger than the uniform field sensitivity of the submicron Hall sensors reported in Ref. [16], and two orders of magnitude larger than that reported in Ref. [17] for micron-scale Hall sensors.

However, the small size scale of our submicron sensors yields a *higher* sensitivity to a local field, so that for biomagnetic tag sensing our devices actually are *more* sensitive. Studies involving micron-scale Hall sensors report detection of single micron-scale magnetic labels [17], and Ref. [5] predicts possible detection of single 250 nm labels with comparable micron-scale GMR sensors. Using our numerical model along with the noise measurements, we can make estimates for the sensitivity of the submicron GMR devices in biological applications. From the white noise level in Fig. 7(a), the response in Fig. 3(c), and the fit model for the dipole field from the SPM tip, we calculate a noise level for a dipole 100 nm above the GMR sensor of  $2 \times 10^{-16} \text{ emu}/\sqrt{\text{Hz}}$ . If we assume a 50 nm thick passivation layer on the sensor surface, then a commercially available 100 nm diameter biomagnetic label, with a dipole moment of  $2 \times 10^{-16} \text{ emu}$  [15],<sup>1</sup> would be situated 100 nm above the sensor surface, and would be at the noise level of the sensor in a 1 Hz bandwidth. Furthermore, a single 200 nm diameter biomagnetic label, with a dipole moment of  $2 \times 10^{-15} \text{ emu}$  [15],<sup>1</sup> could be detected with a position sensitivity of 93 nm in a 1 Hz bandwidth; its presence could be detected with a SNR of 10 in a 1 Hz bandwidth. These results are quite promising, indicating that submicron GMR devices offer highly sensitive detection for biological applications, with the ability to sense single nanoscale labels.

We could further increase the sensitivity by using on-chip resistance bridges as well as ‘flux pipes’ to concentrate the field lines [3,11]. These techniques have already been shown to greatly improve GMR sensor performance in other applications and could no doubt benefit biological application as well [11]. Such techniques, combined with submicron sensors, could push the envelope of sensitivity well into the sub-10 nm particle detection regime.

#### 4. Conclusion

We have fabricated submicron GMR sensors and evaluated them for use as biological sensors. We employed a new scheme for testing such devices in this particular application, and we developed a simple model that allowed us to validate our results as well as make estimates for the sensitivity of the devices in real biological studies. We have shown that the devices have a sensitivity of  $2 \times 10^{-16} \text{ emu}/\sqrt{\text{Hz}}$  for magnetic labels situated 100 nm above the sensor surface.

At this sensitivity the sensor is capable of detecting a single 200 nm magnetic analyte label, offering the possibility for single analyte counting in solution. Furthermore, we believe we could further increase the sensitivity of these sensors using standard technological schemes. These devices offer very sensitive biological particle detection, opening up new avenues for research.

#### Acknowledgements

The authors acknowledge support by the University of California Biotechnology Grant. We thank Bob Hill for processing support.

#### References

- [1] M.N. Baubich, J.M. Broto, A. Fert, F.N.V. Dau, F. Petroff, Giant magnetoresistance of (00 1)Fe/(00 1)Cr magnetic superlattices, *Phys. Rev. Lett.* 61 (1988) 2472–2475.
- [2] D.R. Baselt, G.U. Lee, M. Natesan, S.W. Metzger, P.E. Sheehan, R.J. Colton, A biosensor based on magnetoresistive technology, *Biosens. Bioelectron.* 13 (1998) 731–739.
- [3] M. Tondra, M. Porter, R. Lipert, Model for detection of immobilized superparamagnetic nanosphere assay labels using giant magnetoresistive sensors, *J. Vac. Sci. Tech. A* 18 (2000) 1125–1129.
- [4] J. Schotter, P.B. Kamp, A. Becker, A. Pühler, D. Brinkmann, W. Schepfer, H. Brühl, G. Reiss, A biochip based on magnetoresistive sensors, *IEEE Trans. Magn.* 38 (2002) 3365–3367.
- [5] H.A. Ferreira, D.L. Graham, P.P. Freitas, J.M.S. Cabral, Biodetection using magnetically labelled biomolecules and arrays of spin valve sensors, *J. Appl. Phys.* 10 (2003) 7281–7286.
- [6] R.S. Molday, D. Mackenzie, Immunospecific ferromagnetic iron-dextran reagents for the labeling and magnetic separation of cells, *J. Immunol. Meth.* 52 (1982) 353–367.
- [7] M. Zborowski, C.B. Fuh, R. Green, L. Sun, J.J. Chalmers, Analytical magnetapheresis of ferritin-labeled lymphocytes, *Anal. Chem.* 67 (1995) 3702–3712.
- [8] C.B. Kriz, K. Radevik, D. Kriz, Magnetic permeability measurements in bioanalysis and biosensors, *Anal. Chem.* 68 (1996) 1966–1970.
- [9] H.P. Khng, D. Cunliffe, S. Davies, N.A. Turner, E.N. Vulfson, The synthesis of sub-micron magnetic particles and their use for preparative purification of proteins, *Biotechnol. Bioeng.* 60 (1998) 419–424.
- [10] M.M. Miller, P.E. Sheehan, R.L. Edelstein, C.R. Tamanaha, L. Zhong, A DNA array sensor utilizing magnetic microbeads and magnetoelectronic detection, *J. Magn. Magn. Mater.* 225 (2001) 138–144.
- [11] Nonvolatile Electronics Corporation, Eden Prairie, MN.
- [12] Veeco Instruments Inc., Fort Collins, CO.
- [13] Veeco Metrology Group, Santa Barbara, CA.
- [14] S. McVitie, R.P. Ferrier, J. Scott, G.S. White, A. Gallagher, Quantitative field measurements from magnetic force microscope tips and comparison with point and extended charge models, *J. Appl. Phys.* 89 (2001) 3656–3661.
- [15] Micromod Partikeltechnologie GmbH, Rostock-Warnemuende, Germany.
- [16] K.S. Novoselov, S.V. Morozov, S.V. Dubonos, M. Missous, A.O. Volkov, D.A. Christian, A.K. Geim, Submicron probes for Hall magnetometry over the extended temperature range from helium to room temperature, *J. Appl. Phys.* 93 (2003) 10053–10057.
- [17] P.A. Besse, G. Boero, M. Demierre, V. Pott, R. Popovic, Detection of a single magnetic microbead using a miniaturized silicon Hall sensor, *Appl. Phys. Lett.* 80 (2002) 4199–4201.

<sup>1</sup> The dipole moment is given for a 15 Oe magnetizing field.

## **Biographies**

**D.K. Wood** received his BS in physics from NC State University in 2001. He completed his MA in physics at UC Santa Barbara in 2004 and is currently pursuing his PhD there as well. His graduate research focuses on biophysical instrumentation, biomolecular electronics, and radio frequency electronics.

**K.-K. Ni** received her BS in creative studies with a physics emphasis from UC Santa Barbara in 2003. She is currently pursuing a PhD in physics at the University of Colorado, Boulder. Her graduate research is in the field of atomic and molecular physics as well as quantum optics.

**D.R. Schmidt** received his BS in physics from Pennsylvania State University in 1995 and his PhD in physics from UC Santa Barbara in 2000. He is currently employed at JILA, a joint institute of the University of Colorado, Boulder and NIST. He is working in the areas of ultra-low temperature electronic thermometry and sensitive radiation detectors.

**A.N. Cleland** received his BS in engineering physics and his PhD in physics, both from UC Berkeley. He is presently a professor of physics at UC Santa Barbara, a position he has held since 1997. His present research interests include superconducting devices, high frequency mechanical resonators, single-electron physics, and biophysical instrumentation.